Received: 2 October 2020 | Revised: 11 February 2021 | Accepted: 23 February 2021 | Published on: 5 April 2021

DOI: 10.1002/qj.4011

Quarterly Journal of the Royal Meteorological Society RMetS

RESEARCH ARTICLE

# Evolution of convective characteristics during tropical cyclogenesis

**Gerard Kilroy**

Meteorological Institute, Ludwig Maximilians University of Munich, Munich, Germany

**Correspondence**
G. Kilroy, Meteorological Institute, Ludwig-Maximilians University of Munich, Theresienstr. 37, Munich 80333, Germany.
Email: gerard.kilroy@lmu.de

**Funding information**
German Research Council (Deutsche Forschungsgemeinschaft), Grant/Award Number: KI-2248

**Abstract**

Four idealized, high-resolution (500 m horizontal grid spacing), numerical simulations are used to investigate the evolution of convective structures during tropical cyclogenesis. The simulations all begin with a weak initial axisymmetric cloud-free vortex in a quiescent environment, but differ in the moisture level of the initial sounding and whether or not ice microphysical processes are considered. Irrespective of experimental setup, there is only a short period where shallow or congestus clouds dominate. The shallow cloud phase is slightly extended with the drier initial environmental sounding. The composite structure of the convective elements sampled changes markedly throughout the genesis period. For much of the genesis phase, vertical profiles of the mean convective cell show significant amounts of anticyclonic vorticity produced in cells in the inner core. Towards the end of the genesis phase, there is a large increase in the production of cyclonic vertical vorticity in inner-core convection, and cyclonic vorticity becomes dominant at low-mid levels. The evolution from roughly equal strength vertical profiles of cyclonic/anticyclonic vorticity at low-mid levels to profiles where cyclonic vorticity dominates occurs at relatively low system wind speeds ($V_{max}$ less than 10 m·s$^{-1}$). This finding indicates a change in the structure of vortical convection prior to rapid intensification. In outer-core convection, there are roughly equal strength vertical vorticity dipoles produced throughout the genesis period.

**KEYWORDS**

convection, cyclogenesis, hurricane, tropical cyclone

## 1 | INTRODUCTION

Advances in the state of knowledge of tropical cyclones are reviewed periodically by World Meteorological Organization (WMO) sponsored workshops on tropical cyclones (McBride, 1995; Tory and Montgomery, 2006; Tory and Frank, 2010; Montgomery and Smith, 2011; Tang *et al.*, 2020). In these workshops, the problem of tropical cyclogenesis has been considered separately from that of tropical cyclone intensification as the basic processes involved were thought to be different (e.g., WMO, 1995). Montgomery and Smith (2011) first questioned the idea that the

processes involved in tropical cyclone genesis are somehow different from that of intensification. They suggested that the processes by which deep convection aggregates to build an incipient proto-vortex should be the same as those by which this aggregation continues to build the tropical cyclone as it intensifies. Recently, our group has carried out idealized, three-dimensional, high-resolution numerical model simulations of genesis and intensification that provide strong support for the suggestion that the processes are similar (Kilroy *et al.*, 2017a, 2017b; 2018, Kilroy and Smith, 2017).

## 1.1 | Observations

For a long time, tropical cyclogenesis research was hampered by a lack of observational data as genesis occurs typically over the data-sparse tropical oceans. Research on genesis received a huge boost from data obtained in two significant field experiments: the Tropical Cyclone Structure (TCS08) experiment over the Western North Pacific in August–September 2008 (Elsberry and Harr, 2008) and the Pre-Depression Investigation of Cloud Systems in the Tropics (PREDICT) experiment over the Atlantic and Caribbean region in 2010 (Montgomery *et al.*, 2012).

Radar and satellites provide important sources of observations during genesis. The structure of an individual intense convective cell during the genesis of Hurricane Ophelia (2005) was investigated in detail by Houze *et al.* (2009). Radar data showed a 10 km wide, 17 km deep updraught with a vertical velocity maximum of 20 $m \cdot s^{-1}$. Other studies investigated the evolution of convective structure on different days. Rogers *et al.* (2020) noted a transition in the mass flux profile from top heavy to bottom heavy during the genesis of a storm that developed in moderate shear. Airborne Doppler radar observations from the TCS08 experiment have been used to compare convective structure on different days (Bell and Montgomery, 2010). More recently, the mesoscale processes leading to the tropical cyclogenesis of Hurricane Karl (2010) were investigated by Bell and Montgomery (2019). They found that the convective cycle was responsible for the low-mid level development of the vortex, rather than a sustained lowering of the convective mass flux from increased stabilization. While these studies and experiments provided insightful data on the structure of convection and the incipient pouch-like precursor disturbance, only limited data were obtained on the vertical structure and the evolution of convective structure during genesis.

Other observational studies argued about the importance of changes in convective strength during the genesis phase. Jiang (2012) showed a relationship between intense convection in the inner core and vortex intensity change. They found that the rate of intensification appears to be influenced by convective activity in the inner core. However, they suggested that intense hot towers are not necessary for a storm to undergo intensification. Similarly, Leppert *et al.* (2013) showed that during genesis the coverage by convection increases, while the convective intensity decreases near the onset of rapid intensification (RI). A similar result was also found by Tao and Jiang, (2015). However, Wang (2018), in a study of more than 150 named Atlantic storms, found that convective intensity or area is not a key feature of convection for tropical cyclogenesis. Zawislak and Zipser (2014) agreed that there does not appear to be anything special about strong convection occurring in the day before genesis. The most important feature is that the convection organizes near the pouch centre prior to intensification (Zawislak, 2020). Indeed, Chang *et al.* (2017) showed using satellite data that a major difference between developing and non-developing systems was persistent bouts of convection near the circulation centre. They showed that multi-day convective bursts occurred in 67.5% of the 80 developing cases they studied, but only in 13.8% of the 383 non-developing cases.

## 1.2 | Numerical studies

Convective clouds forming in a region with enhanced absolute vertical vorticity, including weak tropical disturbances, amplify the background vertical vorticity by at least an order of magnitude (Saunders and Montgomery, 2004; Fang and Zhang, 2010; 2011; Wissmeier and Smith, 2011; Kilroy and Smith, 2013). The localized regions of enhanced rotation that are produced by convection are found to outlive the cells that produce them (Wissmeier and Smith, 2011).

The importance of deep convection during the genesis period was highlighted in a series of important theoretical and numerical studies before the foregoing field experiments were carried out. In one of the earliest studies, Hendricks *et al.* (2004) investigated a numerical simulation of the genesis of Hurricane Diana (1984). They found that the development of rotating deep convection and the aggregation of the rotation produced in these cells was a vital feature of the genesis process. Further numerical modelling studies have confirmed that rotating deep convection is a prominent feature during both the genesis and intensification stages (Montgomery *et al.*, 2006; 2010; Nguyen *et al.*, 2008; Braun *et al.*, 2010; Wang *et al.*, 2010; Fang and Zhang, 2011; Davis, 2015). Some of these studies suggested that the aggregation and axisymmetrization process may be explained simply by barotropic dynamics. Recently, however, Kilroy *et al.* (2017a) showed that the merger dynamics was dominated by the system-scale

inflow induced by the collective effects of deep convection, which converges the locally enhanced rotation produced by the convection.

## 1.3 | Isolated convection in a vortical environment

The studies by Hendricks *et al.* and others recognized that, in the presence of vertical shear, convection produces localized regions of anticyclonic vertical vorticity. It was suggested that barotropic dynamics would provide an explanation for the expulsion of this anticyclonic vorticity from the inner-core region, the presumption being that the barotropic dynamics would dominate the presence of system-scale inflow. If the system-scale inflow dominates the barotropic dynamics of expulsion, the anticyclonic anomalies would be carried towards the circulation centre also (Fang and Zhang, 2011).

As a preliminary to further investigating the foregoing processes, it seemed necessary to gain a more complete understanding of the vortical structures produced by deep convection. This perceived need motivated a series of studies (Kilroy and Smith, 2013; 2014, Kilroy *et al.*, 2014) that investigated idealized, high-resolution (horizontal grid spacing 250 m) numerical simulations of isolated convective systems growing in tropical-cyclone-like environments[1]. In an environment with tropical-cyclone-like vertical wind shear (uni-directional and/or directional), it was shown that convection produces dipole patterns of vertical vorticity, including a reversal in sign of the dipole with height. These vorticity dipoles are produced by the tilting of background horizontal vorticity into the vertical, as well as by stretching of existing ambient vorticity. Since the anticyclonic vorticity anomalies can be of equal strength and do not decay more quickly than the cyclonic anomalies, these studies raised questions about the role of anticyclonic vorticity anomalies in the formation of a system-scale cyclonic monopole.

An answer to these questions was offered in a follow-up study by Kilroy and Smith (2016, hereafter KS16), who investigated the generation and evolution of vertical vorticity by deep convection in a warm-cored vortex of near tropical storm strength. The previous suite of idealized studies described above investigated single clouds evolving in a small domain where the background wind shear, either horizontal or vertical, did not vary across the domain. In contrast, KS16 investigated single clouds developing in a large-scale balanced vortex where the dynamic and thermodynamic fields vary with distance from the storm centre. As in the previous idealized studies, convection is initiated by thermal perturbations. These perturbations were located at different radii from the vortex axis. It was found that convection occurring near the vortex centre is weaker than convection occurring closer to the radius of maximum winds because of lower convective available potential energy (CAPE) near the vortex centre. They found also that there are significant differences in the structure of the vorticity anomalies produced at different radii. Convection developing near or at the circulation centre, where the vertical shear associated with the vortex is weak, produces vorticity anomalies that have the structure of a cyclonic monopole and generates little anticyclonic vorticity. These anomalies are produced largely by stretching of background vertical vorticity. At larger radii, near and beyond the radius of maximum tangential wind, vertical vorticity dipoles are generated largely by tilting of background horizontal vorticity. Further, these dipoles also reverse in sign with height.

The results of KS16 indicate that convection near the circulation centre does not generate appreciable anticyclonic vorticity so that there is no need to provide an explanation of how to expel this vorticity. Since the study focused on the evolution of only a single cloud and the length of the simulation was limited to the life cycle of this cloud, the question remains to what extent the findings therein can be applied to an evolving vortex with many clouds, where there is presumably an interaction between the evolving field of convective cells and the pre-depression environment. The question is: to what extent can the findings therein be applied to understand the structure of convectively generated vertical vorticity in an evolving vortex where convection is not forced by artificial thermal perturbations? An answer to this question is expected to lead to a better understanding of the vorticity aggregation process.

## 1.4 | The rotating convection paradigm

To interpret the intrinsically three-dimensional nature of tropical cyclone intensification called for a new conceptual model that accounts for the inherently stochastic, three-dimensional nature of deep convection. This need led to the development of the so-called "rotating convection paradigm," which is summarized by Smith and Montgomery (2016) and reviewed in more detail in Montgomery and Smith (2017). A comparison of this paradigm

[1]Both unidirectional and directional boundary-layer-type wind profiles were used in these studies. The unidirectional shear profile comprised decreasing tangential winds with height above the boundary layer, and increasing tangential winds with height below, mimicking the tangential wind profile in a tropical cyclone, including the effects of frictional loss of momentum near the surface. For directional shear, an Ekman-type boundary-layer wind profile was employed.

with prominent earlier ones, which all assumed axial symmetry, was presented by Montgomery and Smith (2014). As first shown by Kilroy *et al.* (2017a), the rotating convection paradigm provides a conceptual framework for understanding the genesis process also.

The rotating convection paradigm is usually illustrated in the context of the prototype problem for tropical cyclone intensification, which relates to the spin-up of an initially balanced, axisymmetric, cloud-free, conditionally unstable, baroclinic vortex of near tropical storm strength in a quiescent tropical environment on an $f$-plane. A key element of the paradigm is the presence of sustained deep convection in a region of enhanced background rotation over a warm ocean. In broad terms, the convection not only enhances the vertical vorticity locally by stretching, but the collective effects of convection lead to a vortex-scale overturning circulation that converges cyclonic absolute vorticity in the lower half of the troposphere. By Stokes' theorem, this convergence leads to an increase of circulation about horizontal loops of fixed radii encircling the convection or within the convective region and thereby the mean tangential wind speed about these loops. The sustenance of the convection requires evaporation of warm sea water to maintain convective instability.

### 1.5 | The role of cumulus congestus in genesis

On the basis of a numerical simulation of a real storm, Wang (2014a) suggested that, from a thermodynamic viewpoint, tropical cyclone genesis can be viewed as a two-stage process. The first stage is a gradual process of moisture preconditioning, in which "cumulus congestus plays a dominant role in moistening the lower to middle troposphere and spinning up the near-surface circulation prior to genesis." Once the environment becomes unstable enough, the second stage can begin in which "deep convection plays a key role in moistening the upper troposphere and intensifying the cyclonic circulation over a deep layer." The proposed dynamical role of congestus convection in "spinning up the near-surface circulation prior to genesis" merits further investigation as such spin-up would need to be accompanied by organized outflow at levels where the congests detrain. Such outflow should be apparent in azimuthally averaged radial flow fields, but this has not been found in any of our previous work (Kilroy *et al.*, 2017a; 2017b; 2018 etc.). As the majority of these simulations started with a relatively moist pre-hurricane Karl environment as the initial sounding, there is a possibility, worth exploring, that they may have bypassed the cumulus congestus moistening phase and thereby any dynamical effects related to this stage.

### 1.6 | The present study

In her simulation of Tropical Cyclone Fay (2008), Wang (2014a) examined the statistics of deep convection and of stratiform regions produced by deep convection. A similar analysis is carried out here for the two idealized control simulations reported by Kilroy *et al.* (2017a; 2018) and in repeats of these simulations using a drier initial sounding. In particular, I compare the statistics of deep convection in the warm rain only simulation with the statistics when ice microphysical processes are included. Another goal of this study is to examine in detail the evolution of the structure of deep convection that develops in these simulations.

Finally, I carry out an analysis of the statistics of vertical vorticity anomalies at different times and in different regions during genesis. The goal is to examine to what extent the findings of KS16 can be applied to understanding vertical vorticity production throughout the genesis period. This analysis is accompanied by a statistical analysis of vertical vorticity production by the clouds and of the vertical mass flux carried by them at different stages of vortex evolution. It is hoped that such an analysis will contribute to understanding the controls on the low-level convective mass flux and thereby the ability of the convection to ventilate the mass that converges in the boundary layer (e.g., Kilroy *et al.*, 2016). This is an exceedingly important question, but it may be that progress in answering it satisfactorily will be incremental.

The manuscript is organized as follows. A description of the numerical model is given in Section 2, and an explanation of the configuration of the experiments is described in Section 3. An overview of these simulations is presented in Section 4. A statistical analysis of convection during the genesis period is presented in Section 5, while the evolution of the vertical structure of convection is investigated in Sections 6 and 7. Simulations with higher temporal resolution are analysed in Section 8. The conclusions are given in Section 9.

## 2 | THE NUMERICAL MODEL

The simulations presented here have the same configuration as those presented in Kilroy *et al.* (2017a; 2018). The numerical model used is CM1 version 16, a non-hydrostatic and fully compressible cloud model (Bryan and Fritsch, 2002). The simulations relate to the evolution of an initially weak, cloud-free, symmetric vortex with no background flow on an $f$-plane. As described in Kilroy *et al.* (2017a; 2018), the domain is $3,000 \times 3,000$ km in size with variable horizontal grid spacing reaching 10 km near the domain boundaries. The inner $300 \times 300$ km has a uniform horizontal grid spacing

of 500 m. In all experiments presented, genesis occurs inside the region of uniform horizontal grid spacing. There are 40 vertical levels extending to a height of 25 km, with seven grid levels located in the lowest 1 km. The vertical grid spacing expands gradually from 50 m near the surface to 1,200 m at the top of the domain. The simulations are carried out on an $f$-plane with the Coriolis parameter $f = 2.53 \times 10^{-5}$ s$^{-1}$, corresponding to 10°N. Surface fluxes of heat and moisture are included in all simulations. The sub-grid turbulence scheme used is the model option *iturb* = *3*, a parameterized turbulence scheme (Bryan and Rotunno, 2009), which is based on the formulation of Blackadar (1962). This scheme requires the user to specify the horizontal and vertical mixing lengths, which are set to $l_h = 700$ m and $l_v = 50$ m, respectively. These values are close to those recommended by Bryan (2012) to produce realistic hurricane structure. For simplicity, this mixing length is assumed constant in both space and time. For the warm-rain simulations a simple warm-rain scheme is used in which rain has a fixed fall speed of 7 m·s$^{-1}$. This is the Kessler microphysics scheme. For the simulations with ice microphysics, the Morrison microphysics scheme is employed (Morrison *et al.*, 2005). This is the CM1 default option for a microphysics scheme.

Radiative effects are represented by adopting a simple Newtonian cooling approximation, which relaxes back to the reference sounding, capped at a magnitude of 2 K per day, following Rotunno and Emanuel (1987). A Rayleigh damping layer is added at heights above 20 km to suppress the artificial reflection of internal gravity waves from the upper boundary. Rayleigh damping is applied within 100 km of the lateral boundaries, which are rigid walls. The calculations here are carried out for a period of 108 hr. In one simulation with ice microphysics, genesis takes longer to occur, so this simulation is carried out for a period of 150 hr.

## 2.1 | Initial vortex

The structure of the initial vortex is shown in Figure 1. As described in Kilroy *et al.* (2020), it is axisymmetric and warm-cored with a maximum tangential wind speed of 5 m·s$^{-1}$ at the surface. The initial temperature field is in thermal wind balance and is determined using the method described by Smith (2006). The initial vortex is baroclinic, and the tangential velocity profile is given by: $v(r) = v_1 s \exp(-\alpha_1 s) + v_2 s \exp(-\alpha_2 s)$, where $s = r/r_m$ and $r_m$, $v_1$, $v_2$, $\alpha_1$ and $\alpha_2$ are constants[2], chosen to make $v = v_m = 5$ m·s$^{-1}$ at $r = r_m$. The initial tangential wind speed decreases sinusoidally with height, becoming zero at a height of 20 km. The calculations are carried out with the radius of the maximum tangential wind speed, $r_m$, located at 100 km.

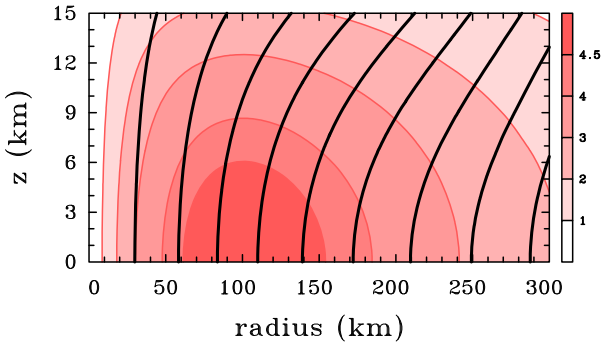


**FIGURE 1** Vertical cross section of the initial vortex structure for all simulations presented herein. Contours as follows: tangential wind as given by shading in the label bar in m·s$^{-1}$. Absolute angular momentum given in black contours every $2 \times 10^5$ m$^2$ ·s$^{-1}$, starting at $1 \times 10^5$ m$^2$ ·s$^{-1}$ [Colour figure can be viewed at wileyonlinelibrary.com]

## 2.2 | Reference sounding

The reference soundings are the same as those used in Kilroy *et al.* (2017a; 2018), and are shown in Figure 2. In brief, the pre-Karl average sounding is a mean of 39 dropsonde soundings obtained on September 12, 2010, during the PREDICT field campaign for the tropical wave-pouch disturbance that eventually became Hurricane Karl on September 16 (see Smith and Montgomery, 2012 and Montgomery *et al.*, 2012 for details). This sounding has a CAPE of 2,028 J·kg$^{-1}$, a convective inhibition of 47 J·kg$^{-1}$ and a total precipitable water (TPW) value of 61 kg·m$^{-2}$. This sounding is moister than the Dunion moist tropical sounding (61 kg·m$^{-2}$ compared with 51.5 kg·m$^{-2}$) (Dunion, 2011), shown as a dashed curve in Figure 2. The Dunion sounding has a slightly larger CAPE (2,104 J·kg$^{-1}$). For a more detailed comparison, see Sections 2 and 3 of Kilroy *et al.* (2017a). The sea surface temperature is 29°C, typical of the Caribbean region at the time.

# 3 | THE EXPERIMENTAL DESIGN AND METHODOLOGY

The experiments that are carried out and certain aspects of the vortex evolution in each case are presented in Table 1. The table includes information about the reference sounding and microphysics scheme used, the length of the gestation period and the number of convective cells

[2]The constants $v_1$ and $\alpha_1$ are determined by the formulae $\alpha_1 = (1 - \mu\alpha_2 \exp(-\alpha_2))/(1 - \mu \exp(-\alpha_2))$, and $v_1 = v_m exp(\alpha_1)(1 - \mu \exp(\alpha_2))$, where $\mu = v_2/v_m$, $\mu = 1.0$ and $\alpha_2 = 0.9$.

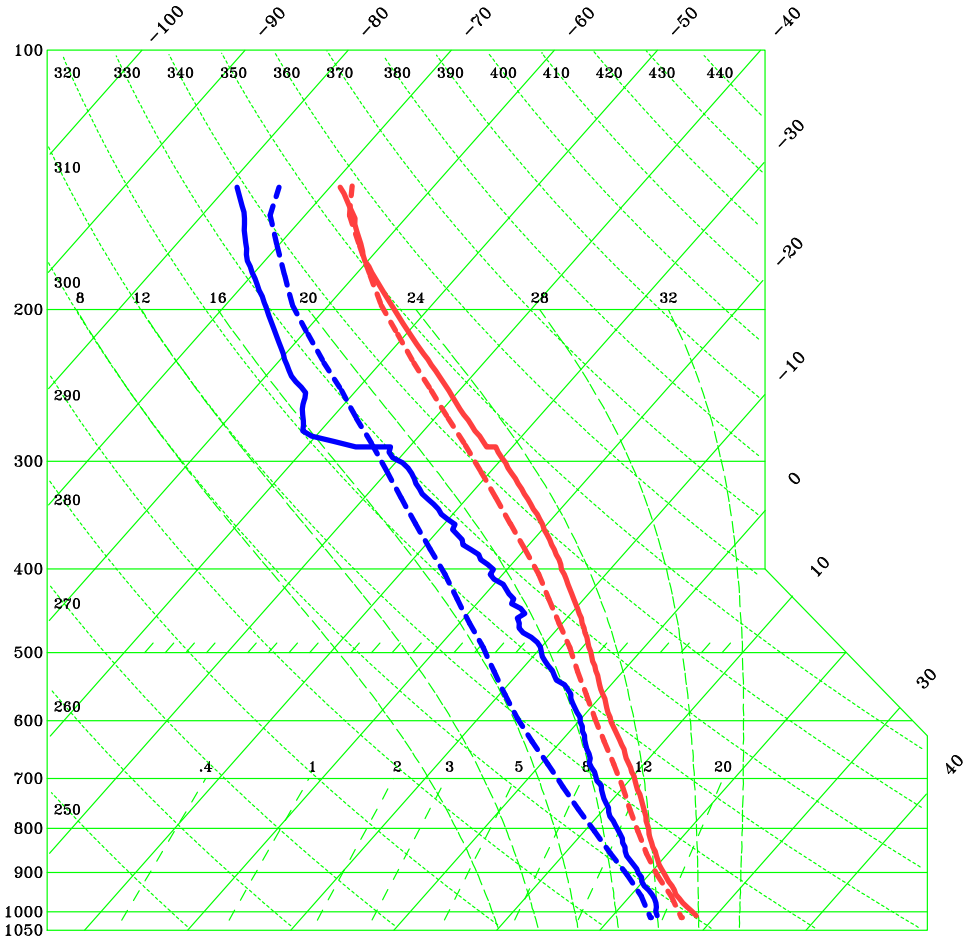


**FIGURE 2** Skew-T log-p diagram showing the temperature (right solid curve) and dew point temperature (left solid curve) of the Karl-pouch sounding. Shown also is the Dunion moist tropical sounding with temperature (right dashed curve) and dew point temperature (left dashed curve) [Colour figure can be viewed at wileyonlinelibrary.com]

**TABLE 1** Details of the experiments studied herein

| Exp | Microphysics | Env. sounding | Genesis completion time | No. clouds inner | No. clouds outer |
|---|---|---|---|---|---|
| E1 | Kessler | Pre-Karl avg. | 49 hr | 4,651 | 25,761 |
| E2 | Kessler | Dunion MT | 59 hr | 4,440 | 26,855 |
| E3 | Morrison | Pre-Karl avg. | 94 hr | 7,277 | 44,312 |
| E4 | Morrison | Dunion MT | 122.5 hr | 7,068 | 51,079 |

*Note:* The thermodynamic soundings are discussed in Section 3. The last two columns provide a count of the number of convective snapshots analysed for both the inner core and the outer region.

analysed. As noted above, the experiments include the original warm-rain (E1) and ice (E3) simulations described by Kilroy *et al.* (2017a; 2018) and reruns of these, but starting from a drier initial sounding (E2 was also briefly described in Kilroy *et al.*, 2017a). The latter sounding is more typical of the tropical cyclone season, rather than the moist pouch-average sounding from pre-Hurricane Karl. The expectation is that the gestation period will be extended, possibly by 1 or 2 days, while the inner-core sounding moistens. One would expect cumulus congestus clouds to play a role in the moistening during the moistening phase.

In this study, genesis is considered to have occurred when the azimuthally averaged tangential wind maximum exceeds 17 $m \cdot s^{-1}$ for the first time[3]. I refer to this

[3]In Kilroy *et al.* (2017a; 2018), the metric they use to signal the end of genesis is what they call the "rapid intensification begin time," where the maximum azimuthally averaged tangential wind speed begins to sharply increase following a period where it increases only slightly. Around this "tipping" point, values of maximum azimuthally averaged tangential wind speed were just below 17 $m \cdot s^{-1}$. Here, a different definition is invoked because in some of the simulations performed it is difficult to eyeball the exact time where the wind speeds start to appreciably increase. Our definition is guided by that given for the

as the genesis completion time. Generally, in the simulations described, RI has begun once this threshold is reached. What constitutes an identifiable convective cell is described below. As the temporal output of the data is only 15 m (cumulus congestus clouds have a lifetime comparable to 15 m, while deep convective cells typically last around 45–90 m), cells are not tracked in time in the analysis performed in Sections 4–7.

## 3.1 | Cloud detection algorithm

A method of identifying convective cells in numerical simulations was described by Terwey and Rozoff (2014). A novel feature of their algorithm, called the Statistical and Programmable Objective Updraft Tracker (SPOUT), is that it tracks three-dimensional clouds in time. The algorithm identifies cells in horizontal slices, and then links cells in each horizontal slice to produce a vertically coherent cloud. The identification and tracking of cells focuses on kinematic fields, rather than on any microphysical aspects of convection. The aim of SPOUT is to provide "better statistical understanding about individual updraft characteristics [that] could allow researchers to form and test hypotheses on the structure, evolution, and microphysical properties of these convective towers." A number of recent studies have utilized SPOUT to analyse convection in rainbands or outer-region convection (e.g., Terwey and Rozoff, 2014; Li and Fang, 2018), or in the inner core during the rapid intensification phase (Harnos and Nesbitt, 2016)[4].

Here I employ a similar method to that in Terwey and Rozoff (2014) to identify clouds, one that I produced myself, but for the analysis in Sections 4–7 I do not track the clouds in time[5]. Therefore, in Sections 4–7, an analysis of snapshots of the convective fields is provided for each 15 min output. Two higher temporal resolution runs are performed also (a repeat of E1 and E2 with 2 min output, the two simulations with the shortest genesis phases), and these simulations are analysed in Section 8. For these simulations, the cloud detection algorithm is able to track cells in time. The motivation for these additional simulations is given in Section 8. For all simulations the analysis is confined to the innermost $300 \times 300$ km of the grid, which has a constant 500 m grid spacing. In all cases examined, vortex spin-up occurs close to the domain centre (for example, see Kilroy *et al.* (2017a)). Most of the convective activity during genesis and the early period of intensification is confined to this innermost uniform grid.

Clouds are first identified by searching the innermost $300 \times 300$ km at all heights for vertical velocities greater than 1.5 m·s$^{-1}$. Any grid point that meets this criterion is identified as a "cloudy area" which is mapped onto a two-dimensional array. This criterion was chosen to be high enough to filter out waves, and also low enough to include most cumulus congestus convection. A three-dimensional column, $10 \times 10$ km in horizontal extent, is centred on each of these cloudy areas. A local maximum in vertical velocity is found within this column, and a cloud at a given time is recorded. The algorithm then analyses the next "cloudy area" and constructs a $10 \times 10$ km column centred over this area also. If the local maximum vertical velocity within this new column is identical to a previous one, the algorithm recognizes this cloud as already identified. The algorithm continues until all "cloudy areas" are analysed. Another constraint is that the distance between two identified clouds must be at least 5 km. Because of this constraint, and the choice of using local maximum vertical velocity to identify clouds, it is possible that some weaker clouds may be lost using this algorithm. For the analysis of 2 min output in Section 8, clouds are tracked in time and analysed only if they are detectable for a minimum of five time steps (10 min).

I define a congestus cell as a cloud with a top between a height of 5 and 9 km (Johnson *et al.*, 1999). Clouds with tops higher than this are considered to be deep convective cells. Clouds with tops lower than 5 km are defined as shallow cumulus. The congestus phase is defined as a period of time where congestus cells dominate deep convective cells in number.

## 3.2 | Variables analysed

The vertical structure of each cloud is obtained by searching for areally averaged values of several variables through a $10 \times 10$ km column from the surface to the domain top. These variables include the relative cyclonic and anticyclonic vertical vorticity, the vertical velocity and vertical

formation of a tropical storm on the National Oceanic and Atmospheric Administration (NOAA) Hurricane Research Division website. A tropical storm is defined as a tropical cyclone with maximum sustained surface winds of 17 m·s$^{-1}$ (34 kt, 39 mph). The difference is that I use only the maximum azimuthally averaged tangential wind instead of total winds, and this maximum can occur at any height.

[4]Studies that do not have the temporal resolution to track clouds in time perform an analysis of snapshots of the convective structure at given times, for example, in numerical simulations of rainband activity (Li and Wang, 2012), or from airborne Doppler radar observations, again focussing on rainband activity (Hence and Houze, 2008; Lee *et al.*, 2008, Eastin and Link, 2009).

[5]To accurately track clouds in time, the temporal output required would need to be less than 5 min (perhaps even as low as 2 min to accurately track shallow and congestus convection). The enormous amount of data that would be produced by having such high temporal resolution for all simulations presented here is a constraint that prevents me from being able to to do this type of analysis, given that one of the longer simulations performed here has an integration time of 150 hr.

mass flux. As the simulations contain no background environmental shear, and the local vortex shear is relatively weak, clouds are rarely tilted so much that they extend outside of this column. This is confirmed by analysing vertical profiles of convective cells (not shown). Absolute maximum and minimum values of several different variables are obtained to provide the basis of the statistical analysis presented later in Section 5.

Inner domain averages of relative humidity, the vertical mass flux per unit area and the relative cyclonic vertical vorticity are constructed by taking a square column average in the inner $50 \times 50$ km. The domain averages highlight the effects of the convective cells in altering the thermodynamics and dynamics of the evolving vortex.

## 4 | VORTEX EVOLUTION

This section provides an overview of vortex evolution in all four simulations, comprising an analysis of some simple metrics including the azimuthally averaged maximum tangential wind speed ($V_{max}$), the radius at which $V_{max}$ occurs ($R_{vmax}$) and the areal fraction of convection in the inner core (inside of a radius of 50 km from the domain centre), and for the outer region (outside a radius of 50 km, but contained within the fine mesh $300 \times 300$ km). These curves are shown in Figure 3. A system averaged view of the evolution is shown also in Figure 4. Here, time–height cross sections are shown of several variables averaged over a column with horizontal dimension $50 \times 50$ km centred over the domain centre.

$V_{max}$ remains close to its initial value in all experiments, with minor fluctuations, until the beginning of the RI phase which occurs sooner in experiments with warm-rain microphysics. For the case with the pre-Karl pouch sounding, E1, the genesis phase, is complete by 49 hr and the RI period commences in which $V_{max}$ increases from about 10 m·s$^{-1}$ to about 70 m·s$^{-1}$ within 36 hr (Figure 3a). A few hours before the RI onset occurs, $R_{vmax}$ decreases to a value of about 10 km (Figure 3b), and remains close to this value for the remainder of the simulation. A similar evolution occurs in the warm-rain simulation with the Dunion MT sounding, E2, although the onset of the RI phase in this simulation occurs about 10 hr later (Figure 3d). With ice microphysics the genesis period takes a lot longer. With the pre-Karl pouch sounding (E3) genesis is complete at 94 hr (Figure 3g), while with the Dunion MT sounding the genesis period takes 122. hr (Figure 3j). In these two cases, $R_{vmax}$ drops to relatively low values up to 10 hr prior to the completion of the genesis phase, whereas it decreases rapidly only a few hours prior in the warm-rain simulations.

Figure 3 (panels c,f,i,l) gives an indication of how convectively active the domain is at a given time. Sustained convection occurring near the circulation centre, which is located at the domain centre, is particularly important dynamically for vortex intensification. The collective effect of this convection is to drive inflow at low-mid levels, which converges cyclonic vertical vorticity. Convective clouds first appear in all simulations at around the same time, from 10–12 hr. Initially, all the convection is located at radii of about 40–75 km from the domain centre (not shown). The convection occurs in this band as a result of frictional convergence of moisture in the boundary layer. The effects of frictional convergence are non-negligible at early times before any convection occurs. A more detailed study of the effects of friction during the genesis period is given in Kilroy *et al.* (2017b). Shortly after this initial burst, convection begins to develop outward in what appears as an outward propagating convective ring (not shown). This convective feature occurs in all four simulations between about 10 and 25 hr. This artificial ring of convection is often discounted in idealized simulation studies and not analysed. However, as it plays a role in moistening the lower troposphere, it is included here.

In both warm-rain calculations, there are several distinct bursts of convective activity in the inner-core region, where the areal coverage of convection increases for a period of about 10–15 hr. In both simulations, there is an increase also in areal fraction towards the end of the genesis phase. In particular, there is a sharp increase in cloud coverage for the last 6 hr in E1. In the inner core, there are periods of reduced activity in both E1 and E2 where the cloud coverage falls to close to zero. Spikes of convective coverage in the inner core coincide with increases in $V_{max}$. In the outer region, there are periods also of reduced convective activity, with a sharp fall in cloud coverage in both simulations during the final 6 hr of the genesis phase.

The situation is rather different in the simulations with ice microphysics (E3 and E4) when compared with the warm-rain cases. For the calculation with the pre-Karl pouch sounding (E3), there are no distinct bursts of convective activity (cloud coverage $> 10\%$) in either the inner core or outer region until the final hours of the genesis period. There is a sharp increase in convective coverage in the inner core from about 10 hr before genesis is complete.

For the case with the Dunion MT sounding (E4), there are more notable fluctuations in convective activity throughout the simulation. There are several spikes in convective coverage in both the inner core and outer region. Following these convective bursts, there are prolonged periods from about 80 hr in which there is reduced activity in the inner core, and from about 85 hr in the outer region. From about 90 hr, the inner-core cloud coverage increases sharply.

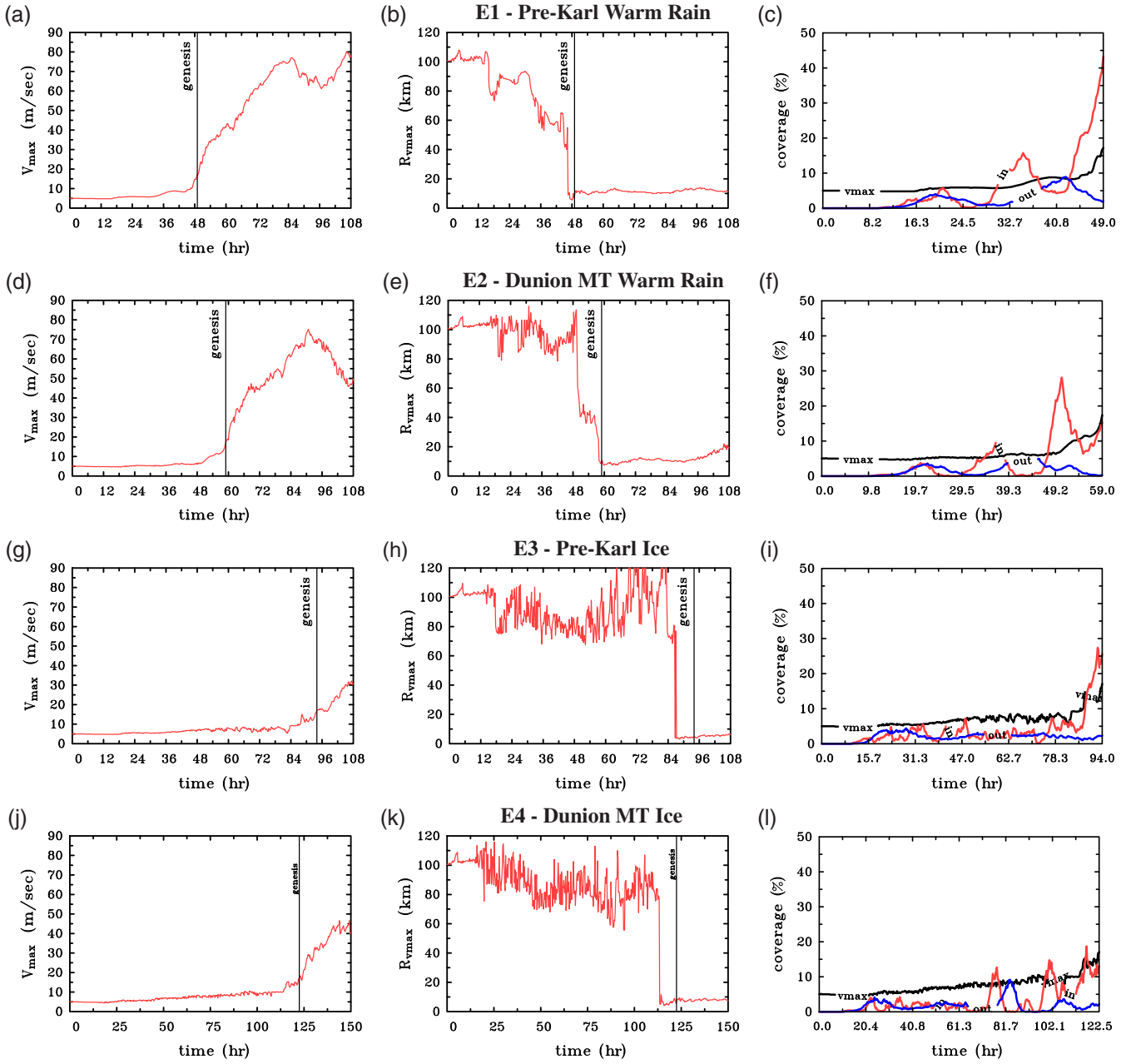


**FIGURE 3** Time series of (a,d,g,j) maximum azimuthally averaged tangential wind speed ($V_{max}$). Panels (b,e,h,k) show the radius $R_{vmax}$ at which the maximum tangential wind speed occurs ($V_{max}$). Panels (c,f,i,l) show cloud areal fractions (in percent). The black curve is $V_{max}$, the red curve labelled "in" shows the areal coverage in the inner core (inside of a radius of 50 km from the domain centre) and the blue curve labelled "out" shows the areal coverage outside of the inner core. Note the shorter time scale for panels (c,f,i,l), which terminates at the time of genesis completion, and the longer time scale for panels (j,k) due to the longer genesis phase in E4 [Colour figure can be viewed at wileyonlinelibrary.com]

Table 1 lists the number of convective snapshots analysed for each experiment in the inner and outer regions. In E1, in which the genesis period is shortest, there are 4,651 convective snapshots analysed in the inner core. Surprisingly, there are slightly fewer cells identified in the inner core of E2, despite the longer genesis period. With substantially longer gestation periods, both the ice simulations E3 and E4 have a much larger number of convective elements than in their warm-rain counterparts. For all simulations, there are substantially more cells analysed in the outer region, as expected (the outer region covers a larger area). These snapshots are the basis for the analysis in Sections 5, 6 and 7.

In agreement with Zawislak and Zipser (2014) and Zawislak (2020), I find an important feature is that the convection organizes near the pouch centre prior to

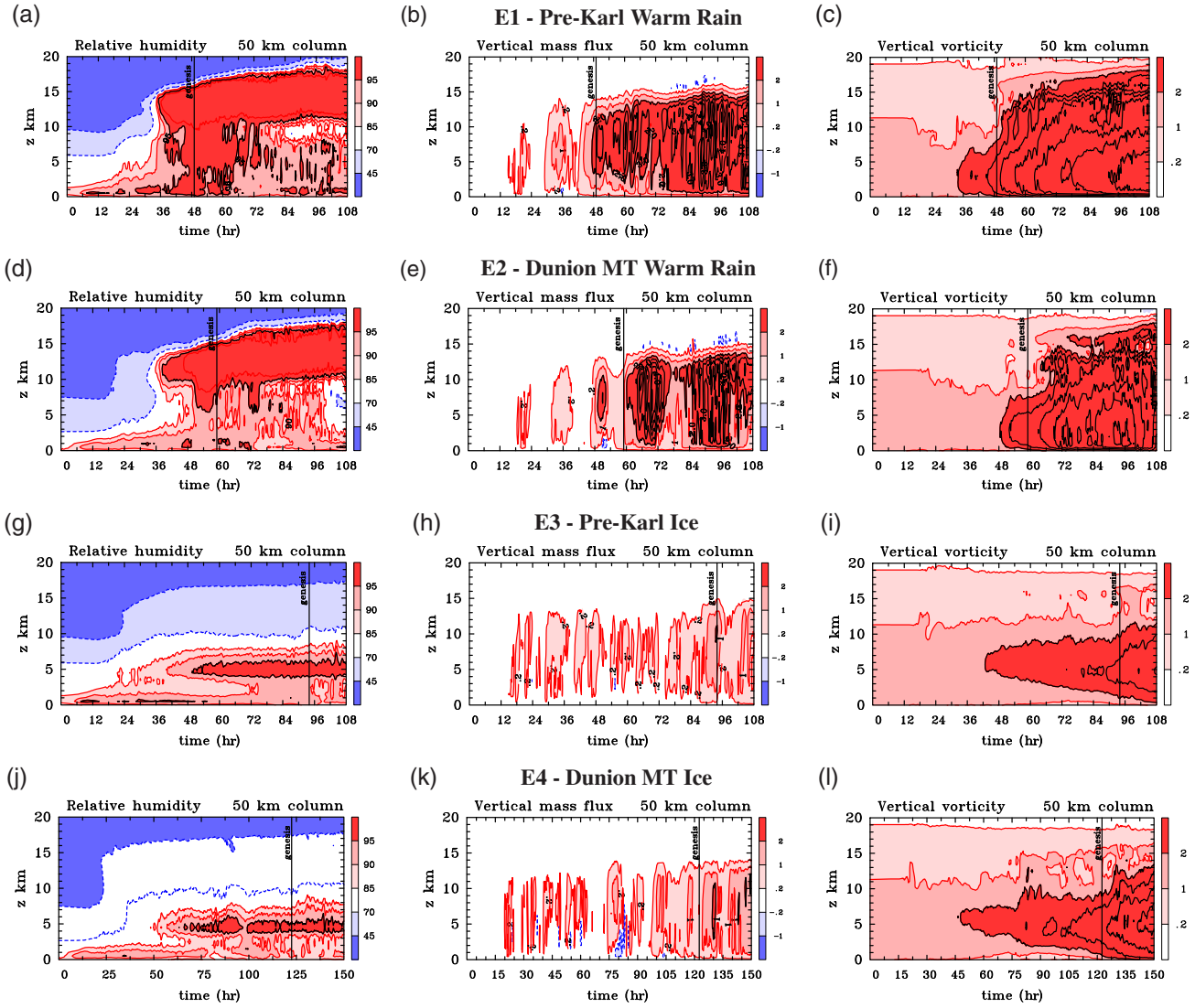


**FIGURE 4** Time–height cross sections of system averaged quantities within a 50 km × 50 km column for all experiments, centred on the domain centre. These quantities include (a,d,g,j) the relative humidity (in percent), (b,e,h,k) the vertical mass flux per unit area (units kg·m$^{-2}$ ·s$^{-1}$) and (c,f,i,l) the relative vertical vorticity (units s$^{-1}$ multiplied by $10^{-4}$). Shading as given in the label bars on the right of each panel. Black contours of vertical mass flux every 1 from 2 kg·m$^{-2}$ ·s$^{-1}$. Black contours of relative vertical vorticity every $1 \times 10^{-4}$ s$^{-1}$ from $2 \times 10^{-4}$ s$^{-1}$. Low values of relative humidity and negative values of vertical mass flux are enclosed by dashed blue contours [Colour figure can be viewed at wileyonlinelibrary.com]

intensification, while outer-region convection tends to decrease in activity. As the convection organizes, there is an increase in the fractional area of convection in the inner core. The increase in fractional area corresponds with an increase in the tangential winds close to the vortex centre. In Section 5, I investigate the intensity of this convection in the period leading into the RI phase.

As in the previous suite of genesis studies (Kilroy *et al.*, 2017a; 2017b; 2018), it is insightful to consider now a system-averaged view of the genesis period. Figure 4 shows cross sections of system-averaged quantities within a column 50 × 50 km, centred at the domain centre for all experiments. The variables shown here include the relative humidity with respect to water vapour, the vertical mass flux per unit area and the vertical component of relative vorticity. As explained in Kilroy *et al.* (2018), it is difficult to compare the relative humidity in the ice and warm-rain simulations because relative humidity is calculated in both sets of simulations with respect to liquid water only. This leads to lower values of relative humidity in the upper troposphere in the ice cases.

In all simulations, the environmental and dynamic conditions (Figure 4) in the inner core evolve significantly during the genesis period. These developments occur during the times $V_{max}$ remains close to its initial value. For E1 and E2, the warm-rain simulations, there is significant

moistening through a depth of at least 15 km. Towards the final 12 hr of the genesis phase, the inner core reaches values of relative humidity of at least 90% through this depth (panels a,d). These results corroborate those of Nolan (2007), who suggested that values of relative humidity must be at least 80% over a significant depth of the troposphere prior to a vortex rapidly developing at mid-levels. In contrast to Nolan (2007), the vortex in both warm-rain simulations develops first at lower levels (panels c,f). In both these simulations, there are a few notable bursts of enhanced positive vertical mass flux associated with convection. After genesis occurs, the mass flux profile is consistently positive in the inner core for the remainder of the simulation.

In the ice simulations, E3 and E4, the evolution is rather different compared with the warm-rain simulations. The evolution is similar to that in Nolan (2007), in that a mid-level vortex intensifies first. The 80% threshold of relative humidity, with respect to liquid water, is reached long before genesis occurs (panels g,j), and a mid-level vortex develops first. This mid-level vortex appears to build downwards with time in both simulations. This development of vorticity in the lower troposphere must be a "bottom up" process, as a net downward transport of vertical vorticity across isobaric surfaces to lower levels violates the important theorem of Haynes and McIntyre (1987)[6]. The mass flux profile shows many bursts of convection in the lead into the onset of RI in both ice simulations.

In general, the conditions in the inner-core region (inside 50 km radius) evolve as a result of the collective effects of convection, which acts to moisten the mid-upper troposphere and to draw air inwards at low and mid levels. The air drawn inward converges background vertical vorticity slowly over time. The changing conditions in the inner core influence the convection that follows. The next sections aim to gain insight into the statistics and vertical structure of the evolving convective elements throughout the genesis period.

## 5 | CONVECTIVE EVOLUTION: STATISTICAL OVERVIEW

In this section, various statistics for the convective snapshots are presented. These statistics include the maximum vertical velocity, maximum relative vertical vorticity and cloud top for each convective cell at each time. They are presented in a contoured frequency distribution (CFD) as a function of time shown in Figure 5. Presented also is a curve showing the evolution of the mean value of these variables.

The CFD for vertical velocity maxima (Figure 5a,d,g,j) shows a brief period where the convection is relatively weak with low cloud tops (panels c,f,i,l). In all cases, the convection becomes deeper and stronger with time. In E1, the mean vertical velocity hovers between 6 and 8 $m \cdot s^{-1}$ following the initial burst, and there is no indication that the mean convective cell weakens or strengthens towards the end of the genesis phase. The mean value of cloud top reaches almost 12 km within about 8 hr of convection first developing. There is brief period starting around 25 hr where the mean cloud top is lower than 8 km. After this period, the mean increases to about 12 km and remains close to this value for the remainder of the genesis period.

The maximum values of vertical vorticity show a general increase during the first period of convection (from about 12–20 hr), but decrease as the first convective burst decays (panel b). From about 30 hr onwards, there is a gradual increase in the mean until the genesis phase ends. This finding is not surprising, as there is a gradual increase with time in the mean cyclonic vorticity of the system scale vortex and cells that develop closer to the end of the genesis phase have more background vorticity to stretch and produce a larger maxima.

In E2, there appears to be a slightly longer initial period of shallow convection than in E1; however, the mean cloud top is close to 10 km only 10 hr after convection commences. There are variations in the mean curves for cloud top and maximum vertical velocity as in E1, marking periods of recovery following periods of vigorous convection. At about 45 hr, there is a period where there is relatively weak shallow convection dominating, and this convection has relatively low values of vertical vorticity. Periods of stronger convection correlate well with higher values of maximum relative vertical vorticity until the last 10 hr where there is a downward trend in the maximum vertical velocity and an upward trend in the maximum vertical vorticity. The reduced vertical velocity during this time appears to be linked to a "lull period" which follows a particularly strong convective burst at about 50 hr (Figures 3f and 4e). The average convective cell in the inner core has a weaker maximum value as new cells develop following the lull.

When ice microphysics are included, the mean vertical velocity maximum is larger than in the warm-rain cases, a result that would be expected because ice processes lead to additional latent heat release and, therefore, additional buoyancy of convection above the freezing level. There is a larger spread in the vertical velocity maxima for these

[6]The issue lies mainly with the idea that vorticity is "built downward over time," which implies a violation of the theorem of Haynes and McIntyre. Additionally, it is unclear how vertical vorticity can be advected downward in a region of mostly upward motion (see inner-core-column averages of vertical mass flux, (Figure 4)). Even if vorticity were advected downwards in down-flow, the flow would diverge near the surface and the vorticity would be diluted.

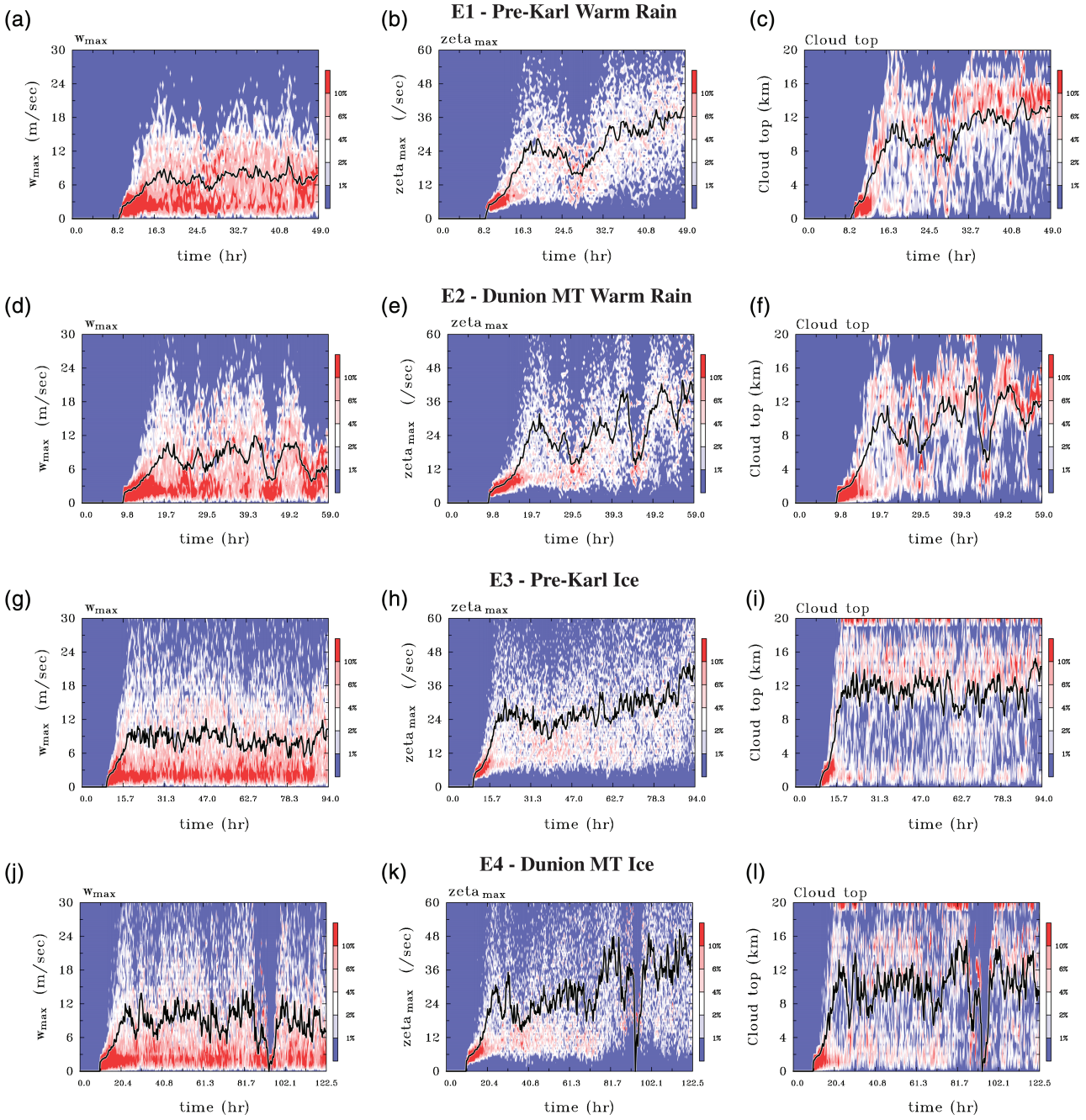


**FIGURE 5** Contoured frequency of several metrics occurring in the inner-core region during the genesis period. These include (a,d,g,j) the maximum vertical velocity in $m \cdot s^{-1}$, (b,e,h,k) the maximum relative vertical vorticity in $s^{-1}$ and (c,f,i,l) the cloud top height in km. Values of vertical vorticity have been multiplied by $10^4$. Label bar units are in percent. The thick black curve gives the mean value at a given time

simulations also. In some individual cases, there are maximum updraught strengths[7] close to 40 $m \cdot s^{-1}$. There is no notable downward trend in the maximum vertical velocity in the final hours of the genesis phase. However, there is a persistent increase in the maximum vertical vorticity values (at times when convection is occurring) from about 40 hr in both E3 and E4.

The big drop in all variables at about 48 and 100 hr in E2 and E4, respectively, coincides with a sudden drop in convective activity (close to zero cells at these times). The cloud coverage in the inner region drops also to almost

[7]While values of 40 $m \cdot s^{-1}$ may seem large, they are typical extreme values found in high-resolution simulations of tropical cyclones. However, values this large are rarely observed, with maximum values of between 20 and 25 $m \cdot s^{-1}$ more typical for tropical environments (Houze *et al.*, 2009).

zero around these times (Figure 3f,l). Similar occurrences are described in Kilroy *et al.* (2018), where convective "lull periods" follow particularly strong convective bursts. The bursts consume the CAPE in the inner region and flood the boundary layer with low values of equivalent potential temperature. There is a brief period where there is no convection in this region while sea surface fluxes of moisture and heat act to restore instability in the inner core.

In all simulations, the cyclonic vorticity maximum in the average cloud increases steadily during the genesis phase. There does not appear to be a significant period of time where cumulus congestus is the dominant cloud mode. The dark-red shaded regions (>10% frequency) generally occur at heights below 4 km, or at heights above 9 km. However, note that this analysis of convective snapshots cannot differentiate between developing cumulonimbus cells and mature shallow or congestus cells.

## 6 | CONVECTIVE EVOLUTION: MEAN VERTICAL STRUCTURE

I turn now to consider the evolution of the mean vertical structure of inner-core convection during different time periods. The main aims of this section are to investigate how the mean vertical structure of convection evolves during the genesis period, and in particular, how the vertical profile of vertical mass flux evolves with time. For all simulations the genesis phase is divided evenly into three separate periods. These periods depict the the early, mid and late stages in the genesis phase. Composites are constructed by averaging the vertical profiles of all the convective elements during these periods. This vertical profile is an areal average of the cell, where $w > 1\ \mathrm{m \cdot s^{-1}}$, in a 10 km column centred on the vertical velocity maximum. Vertical profiles of these means are presented in Figure 6 for all four simulations. The variables presented in these profiles are as follows and are considered in the next subsections in this order: vertical velocity, vertical mass flux, cyclonic relative vertical vorticity and magnitude of anticyclonic relative vertical vorticity.

### 6.1 | Vertical velocity and mass flux profiles

From the vertical profiles of vertical velocity it can be seen there is generally weaker and more shallow convection during the first third of the genesis period (black curves labelled "1" in left panels of Figure 6). The peak mean vertical velocity, which is between 2 and 2.5 $\mathrm{m \cdot s^{-1}}$, occurs at a height of about 2–4 km, except in E3 where it occurs closer to the freezing level. For the second period analysed, during the middle of the genesis period, the peak mean vertical velocity has increased to close to 3 $\mathrm{m \cdot s^{-1}}$ and is located at a height of about 4–5 km in all experiments. The profile has broadened significantly since the first period, with the average convective cell possessing a stronger vertical velocity up to about 16 km height. In the period preceding the completion of the genesis phase, the vertical velocity profile in general broadens in the upper troposphere, an indication that stronger vertical velocities are extending to larger heights. In the warm-rain cases, the peak vertical velocity is weaker than during the middle time period, but in the ice simulations, the peak vertical velocity either remains the same (E3) or becomes stronger (E4).

The corresponding vertical mass flux profiles for all four simulations are shown in panels (b,f,j,n). Raymond *et al.* (2011; 2014) argued that a critical process during the genesis period is a lowering of the convective maximum vertical mass flux from mid-upper levels to low levels. They suggest that this lowering is associated with a mid-level vortex and the related stabilization of the inner core. In all four simulations shown here, the mass flux maximum occurs at low levels (between 2 and 4 km height) during the initial time period analysed. The maximum does not decrease in height with time: in fact, it increases slightly from the first to last period analysed in all simulations. A lowering of the vertical mass flux maximum does not occur even in experiments in which a mid-level vortex develops first. These results suggest that the mid-level vortex and the accompanied stabilization of the inner core are not playing an important role in the genesis process here. An important feature is that the largest positive vertical gradient of the vertical mass flux is always located at low heights in these simulations, corresponding to a favourable situation for development throughout the genesis period.

### 6.2 | Vorticity evolution

Convection forming in a pre-disturbance environment produces vertical vorticity primarily via two processes: (a) stretching of existing vorticity, and (b) tilting of horizontal vorticity into the vertical. The latter process leads to the production of a vertical vorticity dipole. KS16 showed that, in idealized single cloud simulations, the production of vertical vorticity close to the inner core was dominated by stretching of background vertical vorticity, and tilting processes were not important. However, they did not run their simulation long enough to allow for boundary layer friction to significantly change the horizontal shear in the boundary layer.

Figure 6c,g,k,o shows the vertical structure of the areal-averaged cyclonic vertical vorticity, while

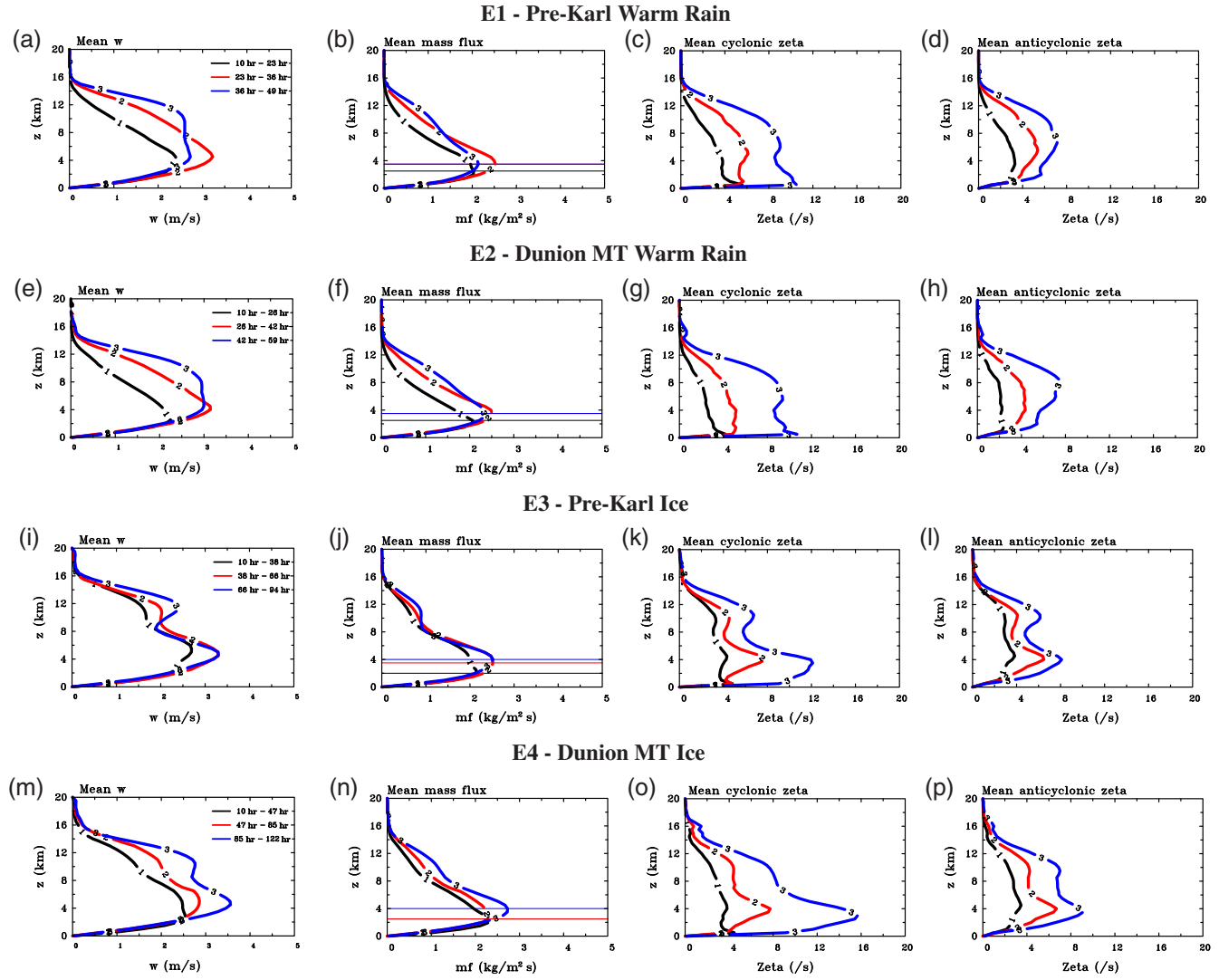


**FIGURE 6** Vertical profiles of time-averaged areal-averaged composites of all inner-core convective cells. (a,e,i,m) vertical velocity in $m \cdot s^{-1}$, (b,f,j,n) vertical mass flux in $kg \cdot m^{-2} \cdot s^{-1}$, (c,g,k,o) cyclonic relative vertical vorticity (units $s^{-1}$ multiplied by $10^{-4}$), and (d,h,l,p) magnitude of anticyclonic relative vertical vorticity (units $s^{-1}$ multiplied by $10^{-4}$). The genesis phase is divided evenly into three different periods. The curve labelled "1" refers to the early time period, "2" the middle time period and "3" the final period. The time periods averaged are given in the left panels. Thin horizontal lines in panels (b,f,j,n) show the height where the vertical mass flux maximum occurs [Colour figure can be viewed at wileyonlinelibrary.com]

Figure 6d,h,l,p shows the magnitude of the areal-averaged anticyclonic vertical vorticity for the three time periods analysed for all experiments. In the first time period, there is little difference between the profiles of cyclonic vertical vorticity and anticyclonic vertical vorticity, with peak values occurring below a height of 4.5 km. However, the mean cyclonic vertical vorticity is larger closer to the surface.

By the middle of the genesis phase, there has been a large increase in magnitudes of cyclonic and anticyclonic vertical vorticity produced by convection. Cyclonic vorticity production is slightly larger than anticyclonic vorticity production from low-mid levels; however, in the upper troposphere values are roughly equal. This is because vortex stretching, which primarily produces cyclonic vertical vorticity, plays a larger role in the low-mid troposphere (where the vertical mass flux gradient is positive), while tilting plays a dominant role in the mid-upper levels. This tilting leads to the production of a roughly equal strength dipole at upper levels. Anticyclonic relative vorticity is produced locally also at mid to upper levels where there is vortex tube dilution due to divergence.

A major development has occurred between the mid-late stages in the genesis process. There has been a large increase in cyclonic vertical vorticity production at low-mid levels in all four cases, with cyclonic vorticity dominating anticyclonic vorticity in convective cells at these heights. In simulations with ice, the largest

increase occurs at about 3 km height. The difference is still small at upper levels. The reason for the dominance of cyclonic vorticity at low levels is the fact that the inflow induced by the collective effects of inner-core convection has concentrated cyclonic vorticity in the inner core, as seen by increases in column average vertical vorticity (Figure 4c,f,i,l). Convection that forms in this region of increased background rotation can stretch this enhanced vertical vorticity further, producing regions of enhanced localized cyclonic vorticity at low-mid levels. The large increase in the mean cyclonic vertical vorticity (and large difference between cyclonic and anticyclonic vorticity) at low-mid levels in the convection occurs when the vortex is still relatively weak ($V_{max}$ less then 10 m·s$^{-1}$), indicating an obvious change in the way that vorticity is produced in convective cells prior to genesis completing.

The large magnitude of anticyclonic vorticity was reported also by Fang and Zhang (2011) and Wang (2014b). Wang (2014b) showed that the cyclonic and anticyclonic vorticity maxima have a similar magnitude throughout the pre-genesis period, but cyclonic vorticity has a larger area coverage. Here there is an obvious difference between the cloud areal-averaged cyclonic and anticyclonic vorticity maxima. The difference from the present study to that of Wang (2014b) is likely due to the different sizes of the inner domains analysed.

### 6.3 | Discussion

A rather surprising result is the relatively large magnitudes of anticyclonic vertical vorticity produced through the depth of the mean convective cell during much of the genesis period. These results suggest that the finding of KS16 that not much anticyclonic vorticity is produced in convection in the inner core does not apply at all times during the genesis period. The relatively large magnitudes of anticyclonic vertical vorticity at lower levels can be explained by the development of horizontal vorticity in the boundary layer and the subsequent tilting of this horizontal vorticity into the vertical. At the initial time, the largest tangential winds occur at the surface; however, in the period before convection occurs (from 0 hr to about 12 hr), there is a reduction in the winds near the surface due to friction. This loss of tangential momentum in the boundary layer produces imbalance that results in inflow. The combination of sheared tangential and radial flow produces a clockwise turning wind hodograph in the boundary layer, or an Ekman-like boundary layer wind profile. Classical studies have detailed the effects of these winds profile on convective structure (Klemp and Wilhelmson, 1978; Schlesinger, 1978; Weisman and Klemp, 1982); however, their focus was on mid-latitude convection and did not include a layer of negative shear above the boundary layer as occurs in a warm-cored vortex. When this extra complication was included, it was found that there is a vertical vorticity dipole that rotates in height in the boundary layer, and then changes sign at some height above the boundary layer (Kilroy and Smith, 2013). With this type of wind profile, there is significant production of anticyclonic vertical vorticity at both the low levels and the mid-upper levels.

In agreement with Kilroy and Smith (2013; 2016), cyclonic vorticity dominates at low-mid levels in the hours leading to the end of the genesis phase. It is at these heights that system scale inflow occurs, so that the convergence of vorticity towards the domain centre will lead to a net increase in system-scale cyclonic vorticity. From Stokes' theorem, an increase of vertical vorticity in a fixed loop around the flow leads to an increase in the circulation around this loop. Because of this vorticity influx, there will be some point in time where the circulation around a fixed loop (located inside the initial $R_{vmax}$) exceeds in strength the circulation at larger radii, and $R_{vmax}$ decreases. The decrease can occur as a jump or it can be more gradual. Following the decrease in $R_{vmax}$, the convection continues to flare in the inner core, and eventually $V_{max}$ reaches a threshold value of 17 m·s$^{-1}$ and the genesis phase is complete.

In summary, the structure of the mean convective element changes markedly throughout the genesis period. Initially, the areally averaged convection is relatively weak. With time, the convection becomes stronger and deeper, with stronger upward motion extending to larger heights. The vertical mass flux maximum does not decrease in height throughout the genesis phase. In fact, there is a slight increase in height with time. An important feature is that there is a large positive gradient of vertical mass flux at low levels at all times, implying a large magnitude of vertical vorticity stretching occurring at low levels. The vertical vorticity profile shows a similar strength magnitude of cyclonic and anticyclonic vorticity during the early and middle phases of the genesis period, but large differences occur at low-mid levels towards the end of the genesis phase. Cyclonic vorticity dominates at low-mid levels where stretching is largest during these later times, although a similar strength cyclonic/anticyclonic profile exists at upper levels where tilting dominates.

## 7 | CONVECTIVE EVOLUTION: OUTER REGION

Here, I consider briefly the evolution of the mean areally averaged vertical structure of outer-region convection at the same time periods as in the previous section. Vertical

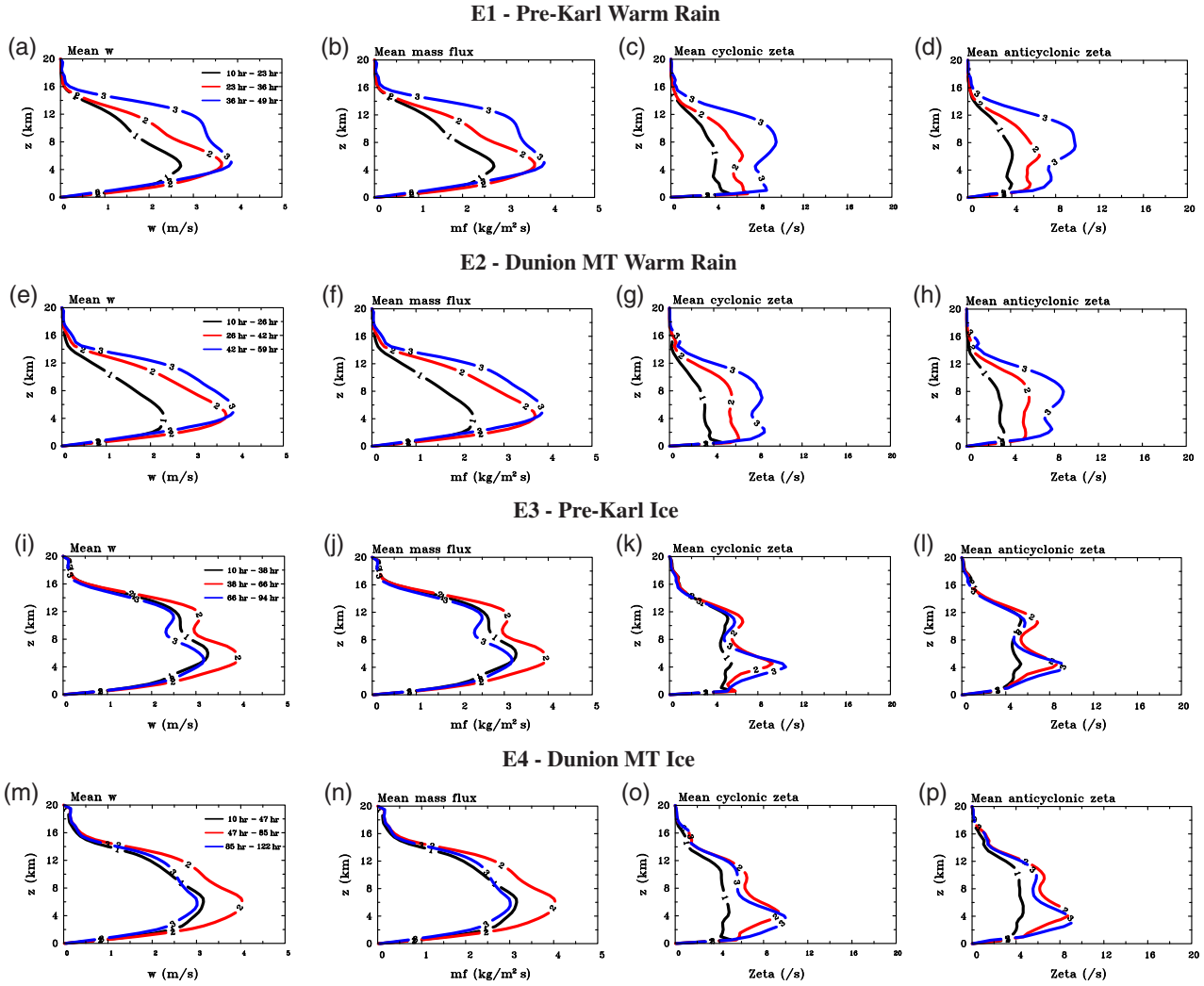


**FIGURE 7** Vertical profiles of time averaged areal-averaged composites of all outer-region convective cells. (a,e,i,m) vertical velocity in $m \cdot s^{-1}$, (b,f,j,n) vertical mass flux in $kg \cdot m^{-2} \cdot s^{-1}$, (c,g,k,o) cyclonic relative vertical vorticity (units $s^{-1}$ multiplied by $10^{-4}$) and (d,h,l,p) magnitude of anticyclonic relative vertical vorticity (units $s^{-1}$ multiplied by $10^{-4}$). The genesis phase is divided evenly into three different periods. The curve labelled "1" refers to the early time period, "2" the middle time period and "3" the final period. The time periods averaged are given in the left panels [Colour figure can be viewed at wileyonlinelibrary.com]

profiles of these means are presented in Figure 7, again for all four simulations.

In all cases, the profiles of vertical velocity and vertical mass flux are similar in both outer-core and inner-core convection, although they are typically larger in magnitude in outer-region convection. In particular, the convective mass flux maximum in outer-region convection is located slightly higher than in inner-core convection. However, the maximum still occurs at relatively low heights at all times, and there is even a slight elevation of the mass flux maximum in the warm-rain simulations. There is, however, a slight decrease in height of the mass flux maximum with time in E3, with little change in E4. The biggest difference between inner- and outer-core convection is in the vertical profiles of vertical vorticity. For outer-region convection, the magnitudes of cyclonic and anticyclonic vertical vorticity generally increase with time, but the difference in the magnitudes of cyclonic and anticyclonic vorticity is minimal just before the genesis period is complete. KS16 found a similar result that convection occurring at large radii produced an almost equal strength vorticity dipole.

## 8 | INVESTIGATION OF CONGESTUS PHASE

In the foregoing analysis of convective snapshots, it was difficult to differentiate between developing deep cumulonimbus cells and mature congestus cells. To be able to determine whether a cell can be classified as congestus or not, higher temporal resolution output data is required.

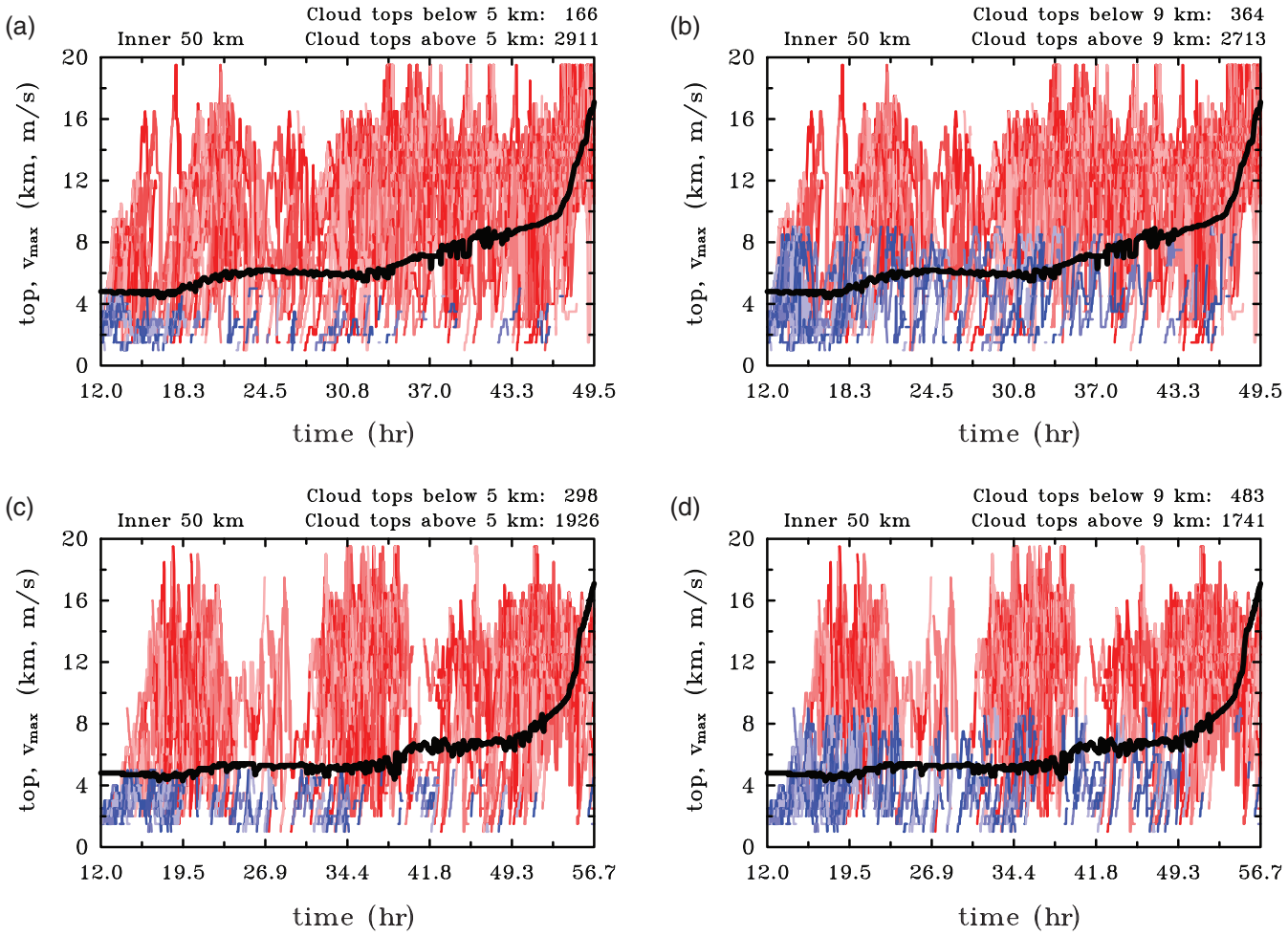


**FIGURE 8** Evolution of cloud tops (using 2 min output) for all clouds (tracked for a minimum of 10 min) that are located within a radius of 50 km from the axis in E1 (panels a,b) and E2 (panels c,d). In panels (a,c), blue curves highlight clouds with tops that never reach above 5 km, and red curves highlight clouds with tops higher than 5 km. In panels (b,d), blue curves highlight clouds with tops that never reach above 9 km, and red curves highlight clouds with tops higher than 9 km. The black curve is $V_{max}$

For this section, E1 and E2 were rerun, but with 2 min data output from the time where convection first develops (at close to 12 hr) to the end of the genesis phase. Unfortunately, such an analysis was not possible for all four simulations because of the immense amount of data output[8]. The following analysis investigates the claim by Wang (2014a) that, from a thermodynamic viewpoint, tropical cyclone genesis can be viewed as a two-stage process. In the first stage, "cumulus congestus plays a dominant role in moistening the lower to middle troposphere and spinning up the near-surface circulation prior to genesis."

Figure 8 shows the evolution of inner-core cloud tops for each cloud identified and tracked in time (for a minimum of 10 min). The left panels highlight clouds that never extend above a height of 5 km (blue curves), with red curves showing cells that have tops above 5 km at some point in their lifetime. These panels display the number of shallow cells that develop. The right panels display clouds that never extend above a height of 9 km (blue curves), with red curves showing clouds with tops above 9 km at some point in their life cycle. The blue curves in these panels display the combined amount of shallow and congestus cells, while red curves display the total number of deep convective cells.

Figure 8a shows that shallow convection in E1 is most prominent in the initial 6 hr period after convection commences. Thereafter, there are few shallow cells observed. In total, there are only 166 shallow cells identified during the genesis phase, compared with 2,911 deeper cells (congestus and cumulonimbus). In panel (b), the blue curves highlight both shallow and congestus cells. Congestus cells are identified throughout the genesis period, although they occur less frequently beyond the initial

[8]In particular, the genesis phase in the ice simulations runs to 94 and 122.5 hr for E3 and E4, respectively.

burst. The total number of congestus cells identified is 198 (364 congestus and shallow cells minus 166 shallow cells). This compares to a total of 2,713 deep convective cells identified.

For E2 (Figure 8c,d), the situation is similar; however, there is a larger amount of shallow cells, which is to be expected in a drier environment. Shallow and congestus convection are most prominent for the 6–10 hr period after convection first flares up. However, there are only 185 identified cumulus congestus cells throughout the genesis period, with the majority of these confined to the first convective burst. In total, 1,741 deep cells are identified.

In summary, there is only a brief period at the beginning of the simulations where shallow clouds are prominent. Further, this shallow cloud phase occurs during the initial burst of ring-like convection, which is an artefact of the method of initialization. These findings do not support the theory of Wang (2014a), who suggested that tropical cyclone genesis can be viewed as a two-stage process. Here, the simulations show that the process of moisture pre-conditioning by relatively shallow convective clouds occurs over a period of only about 6 hr. The analysis suggests that cumulus clouds do not play a dominant role in the dynamics of tropical cyclogenesis beyond this time period in these idealized simulations. It suggests also that there is no need to invoke a two-stage process explanation, provided that the environmental shear is close to zero and the environment is at least as moist as the seasonal average.

The findings here are backed up by an azimuthally averaged analysis (Kiloy *et al.,* 2017; 2018), which showed no outflow signature at heights that one would expect cumulus congestus to detrain. If cumulus congestus played a dominant role during the genesis phase, one should expect to see a signature in these azimuthally averaged fields.

A possible reason for the differences between this study and that of Wang (2014a) is the idealistic nature of the simulations analysed here. While Wang (2014a) investigated a full-physics case of TC Fay (2008), the vortices investigated here evolve in a quiescent environment. It is possible that the inclusion of detrimental environmental conditions such as background vertical shear may lead to a prolongation of the shallow and cumulus congestus phases. The inclusion of background shear would lead to enhanced mixing of environmental air into the developing cells and lead to a possible reduction in updraught height and strength. The effects of shear on the evolution of convection during the genesis phase will be the topic of a future study. Another possibility is that the seasonal average sounding employed here is already moist enough to bypass the congestus phase. In an axisymmetric framework, Tang *et al.* (2016) found a prolongation of the shallow and cumulus congestus phases when the atmosphere is drier initially.

There is a need to further analyse simulations with a more realistic background wind field, or better still, simulations of real life events to verify the ideas presented herein. Real life event simulations should be compared with observations to confirm the role of congestus cells in storms that develop in low shear and relatively moist environments.

## 9 | CONCLUSIONS

I have presented four idealized, high-resolution (500 m horizontal grid spacing), numerical simulations designed to investigate the evolution of convective structure during tropical cyclogenesis. The simulations all begin with a weak initial axisymmetric cloud-free vortex with a maximum tangential wind speed of 5 $m \cdot s^{-1}$. Two simulations were initialized with a relatively moist pre-disturbance environment, the other two with a somewhat drier seasonal mean sounding. Genesis occurs in all simulations, although the length of the genesis period is dependent on both the environmental sounding and the microphysics scheme employed.

Corroborating previous work, the genesis period is about twice as long in cases that include ice microphysical processes when compared with those that have warm-rain physics only. The number of convective elements identified in the inner core for the ice simulations is much larger than in the warm-rain cases, especially in the outer region (outside 50 km radius). Despite the differences in length of the genesis period for simulations with different thermodynamic soundings, the number of convective cells identified is roughly equal, for both the warm-rain cases and the ice cases. The results suggest that the number of convective cells occurring during the genesis period is not important. Cloud areal coverage increases dramatically in the inner core in the hours leading to the end of the genesis phase.

In cases with a drier initial environmental sounding, there is a lengthening of the genesis period by about 12 hr in the case with warm-rain physics, and by about 1 day in the case with ice physics. Irrespective of microphysical scheme and environmental sounding employed, there is not a prolonged period where cumulus congestus clouds dominate, that is, the majority of cloud tops occurring between 5 and 9 km height. Following the onset of convection, there is a period where shallow and congestus convection dominate (cloud tops lower than 9 km). The shallow cloud phase is slightly longer with the more stable initial environmental sounding. This finding does not support the theory of Wang (2014a), who suggested that tropical

cyclone genesis can be viewed as a two-stage process. In these simulations, the process of moisture preconditioning by relatively shallow convective clouds occurs over a very short time period. The conditions in the inner core (inside a radius of 50 km) in these simulations, both for the pre-Karl and Dunion MT environments, become unstable enough on very short time scales, suggesting that cumulus congestus does not play a dominant role in the dynamics of tropical cyclogenesis in a relatively moist unsheared environment. A possible explanation for differences between this study and that of Wang (2014a) is the lack of vertical shear in these simulations, which may play a role in prolonging the length of the shallow cloud or congestus phase.

In all cases examined here, there is no lowering of the inner-core convective maximum vertical mass flux with time. Raymond and Sessions (2007) and Raymond *et al.* (2011; 2014) argued that a critical process during the genesis period is a lowering of the convective maximum vertical mass flux associated with the formation of a mid-level vortex and the stabilization of the inner core. These results suggest that the mid-level vortex and the accompanied stabilization of the inner core is not playing an important role in the genesis process here. An important feature is that the largest positive vertical gradient of the vertical mass flux is always located at low-mid levels, even at early times.

The structure of the average convective element changes markedly throughout the genesis period. At early-mid times in the genesis phase, vertical profiles of the mean convective cell show significant amounts of anticyclonic vorticity produced in cells in the inner core. Towards the end of the genesis phase, there is a large increase in the production of cyclonic vertical vorticity in convection, which becomes dominant at low-mid levels. At upper levels, there is roughly equal strength vertical vorticity dipoles produced throughout genesis. The evolution from roughly equal strength vertical profiles of cyclonic/anticyclonic vorticity at low-mid levels to profiles where cyclonic vorticity dominates occurs at relatively low system wind speeds ($V_{max}$ less than 10 m·s$^{-1}$), indicating a change in the way that vorticity is produced in convective cells prior to the completion of genesis.

As the large-scale conditions in the inner-core region (inside 50 km radius) evolve because of the collective effects of convection, mean cyclonic vorticity in the inner domain increases. Cells developing in regions of enhanced background vorticity stretch this vorticity further and, eventually, due to this enhanced stretching, cyclonic vorticity dominates at low-mid levels (corroborating results of Montgomery *et al.*, 2006, who found a cyclonic vorticity bias at later times in the lower troposphere). It is at these heights that system-scale inflow occurs, so that the flux of vorticity towards the domain centre leads to a net increase of cyclonic vorticity there. From Stokes' theorem, a net increase of vorticity in a fixed loop around the flow leads to an increase in the circulation around this loop. Eventually, enough cyclonic vertical vorticity is converged in the inner core and the vortex intensifies. Soon after, $V_{max}$ increases to the threshold value of 17 m·s$^{-1}$, marking the completion of the genesis phase.

A potential indicator that the genesis phase is near completion is the development of large differences in magnitudes of cyclonic and anticyclonic vorticity in inner-core convection at low-mid levels. This difference does not appear at early-mid times of the genesis phase, nor does it occur at any time in outer-region convection.

## ACKNOWLEDGEMENTS

GK acknowledges financial support for tropical cyclone research from the German Research Council (Deutsche Forschungsgemeinschaft) under grant number KI-2248. I am grateful to Roger Smith and Michael Montgomery for stimulating discussions during an early draft of this manuscript. I thank Zhuo Wang, Brian Tang and the anonymous reviewers for their perceptive comments on early drafts of this manuscript.

Open access funding enabled and organized by Projekt DEAL.

## ORCID

*Gerard Kilroy* https://orcid.org/0000-0002-9240-6555

## REFERENCES

Bell, M.M. and Montgomery, M.T. (2010) Sheared deep vortical convection in pre-depression Hagupit during TCS08. *Geophysical Research Letters*, 37, L06802.

Bell, M.M. and Montgomery, M.T. (2019) Mesoscale processes during the genesis of Hurricane Karl (2010). *Journal of the Atmospheric Sciences*, 76, 2235–2255.

Blackadar, A.K. (1962) The vertical distribution of wind and turbulent exchange in a neutral atmosphere. *Journal of Geophysical Research*, 67(8), 3095–3102.

Braun, S.A., Montgomery, M.T., Mallen, K.J. and Reasor, P.D. (2010) Simulation and interpretation of the genesis of Tropical Storm Gert (2005) as part of the NASA Tropical Cloud Systems and Processes Experiment. *Journal of the Atmospheric Sciences*, 67, 999–1025.

Bryan, G.H. and Fritsch, J.M. (2002) A benchmark simulation for moist nonhydrostatic numerical models. *Monthly Weather Review*, 130, 2917–2928.

Bryan, G.H. and Rotunno, R. (2009) The maximum intensity of tropical cyclones in axisymmetric numerical model simulations. *Monthly Weather Review*, 137, 1770–1789.

Bryan, G.H. (2012) Effects of surface exchange coefficients and turbulence length scales on the intensity and structure of numerically simulated hurricanes. *Monthly Weather Review*, 140, 1125–1143.

Chang, M., Ho, C.H., Park, M.S., Kim, J. and Ahn, M.H. (2017) Multiday evolution of convective bursts during western North Pacific

tropical cyclone development and nondevelopment using geostationary satellite measurements. *Journal of Geophysical Research: Atmospheres*, 122, 1635–1649.

Davis, C.A. (2015) The formation of moist vortices and tropical cyclones in idealized simulations. *Journal of the Atmospheric Sciences*, 72, 3499–3516.

DiGangi, E.A., MacGorman, D.R., Ziegler, C.L., Betten, D., Biggerstaff, M., Bowlan, M. and Potvin, C.K. (2016) An overview of the 29 May 2012 Kingfisher supercell during DC3. *Journal of Geophysical Research: Atmospheres*, 121, 14, 316–14,343.

Eastin, M.D. and Link, M.C. (2009) Miniature supercells in an offshore outer rainband of Hurricane Ivan (2004). *Monthly Weather Review*, 137, 2081–2104.

Elsberry, R. and Harr, P. (2008) Tropical cyclone structure (TCS08) Field experiment scientific basis, observational platforms, and strategy. *Asia-Pacific Journal of Atmospheric Sciences*, 44, 1–23.

Fang, J. and Zhang, F. (2010) Initial development and genesis of Hurricane Dolly (2008). *Journal of the Atmospheric Sciences*, 67, 655–672.

Fang, J. and Zhang, F. (2011) Evolution of multiscale vortices in the development of Hurricane Dolly (2008). *Journal of the Atmospheric Sciences*, 68, 103–122.

Harnos, D.S. and Nesbitt, S.W. (2016) Passive microwave quantification of tropical cyclone inner-core cloud populations relative to subsequent intensity change. *Monthly Weather Review*, 144, 4461–4482.

Haynes, P. and McIntyre, M.E. (1987) On the evolution of vorticity and potential vorticity in the presence of diabatic heating and frictional or other forces. *Journal of the Atmospheric Sciences*, 44, 828–841.

Hence, D.A. and Houze, R.A. (2008) Kinematic structure of convective-scale elements in the rainbands of Hurricanes Katrina and Rita (2005). *Journal of Geophysical Research*, 113, D15108

Hendricks, E.A., Montgomery, M.T. and Davis, C.A. (2004) On the role of 'vortical' hot towers in formation of tropical cyclone Diana (1984). *Journal of the Atmospheric Sciences*, 61, 1209–1232.

Houze, R.A., Lee, W.-C. and Bell, M.M. (2009) Convective contribution to the genesis of hurricane Ophelia (2005). *Monthly Weather Review*, 137, 2778–2800.

Jiang, H. (2012) The relationship between tropical cyclone intensity change and the strength of inner-core convection. *Monthly Weather Review*, 140, 1164–1176.

Johnson, R.J., Rickanbach, T.M., Rutledge, S.E., Ciesielski, P.E. and Schubert, W.H. (1999) +Trimodal characteristics of tropical convection. *Journal of Climate*, 12, 2397–2418.

Kilroy, G. and Smith, R.K. (2013) A numerical study of rotating convection during tropical cyclogenesis. *Quarterly Journal of the Royal Meteorological Society*, 139, 1255–1269.

Kilroy, G., Smith, R.K. and Wissmeier, U. (2014) Tropical cyclone convection: the effects of ambient vertical and horizontal vorticity. *Quarterly Journal of the Royal Meteorological Society*, 140, 1756–1770.

Kilroy, G. and Smith, R.K. (2014) Tropical-cyclone convection: the effects of a vortex boundary layer wind profile on deep convection. *Quarterly Journal of the Royal Meteorological Society*, 141, 714–726.

Kilroy, G. and Smith, R.K. (2016) A numerical study of deep convection in tropical cyclones. *Quarterly Journal of the Royal Meteorological Society*, 142, 3138–3151.

Kilroy, G., Smith, R.K. and Montgomery, M.T. (2016) Why do model tropical cyclones grow progressively in size and decay in intensity after reaching maturity?. *Journal of the Atmospheric Sciences*, 73, 487–503.

Kilroy, G. and Smith, R.K. (2017) The effects of initial vortex size on tropical cyclogenesis and intensification. *Quarterly Journal of the Royal Meteorological Society*, 143, 2832–2845.

Kilroy, G., Smith, R.K. and Montgomery, M.T. (2017a) A unified view of tropical cyclogenesis and intensification. *Quarterly Journal of the Royal Meteorological Society*, 143, 450–462.

Kilroy, G., Smith, R.K. and Montgomery, M.T. (2017b) The role of boundary layer friction on tropical cyclogenesis and intensification. *Quarterly Journal of the Royal Meteorological Society*, 143, 2524–2536.

Kilroy, G., Smith, R.K. and Montgomery, M.T. (2018) The role of heating and cooling associated with ice processes on tropical cyclogenesis and intensification. *Quarterly Journal of the Royal Meteorological Society*, 144, 99–114.

Kilroy, G., Smith, R.K. and Montgomery, M.T. (2020) An idealized numerical study of tropical cyclogenesis and evolution at the Equator. *Quarterly Journal of the Royal Meteorological Society*, 146, 685–699.

Klemp, J.B. and Wilhelmson, R.B. (1978) The simulation of three-dimensional convective storm dynamics. *Journal of the Atmospheric Sciences*, 35, 1070–1096.

Lee, W.C., Bell, M.M. and Goodman, K.E.J.r. (2008) Supercells and mesocyclones in outer rainbands of Hurricane Katrina (2005). *Geophysical Research Letters*, 35, L16803

Leppert, K.D., Cecil, D.J. and Petersen, W.A. (2013) Relation between tropical easterly waves, convection, and tropical cyclogenesis: a Lagrangian perspective. *Monthly Weather Review*, 141, 2649–2668.

Li, Q. and Wang, Y. (2012) A comparison of inner and outer spiral rainbands in a numerically simulated tropical cyclone. *Monthly Weather Review*, 140, 2782–2805.

Li, Q. and Fang, Q. (2018) A numerical study of convective-scale structures in the outer cores of sheared tropical cyclones: 1. updraft traits in different vertical wind shear magnitudes. *Journal of Geophysical Research: Atmospheres*, 123, 12,097–12,116.

Lucas, C., Zipser, E.J. and Lemone, M.A. (1994) Vertical velocity in oceanic convection off tropical Australia. *Journal of the Atmospheric Sciences*, 51, 3183–3193.

McBride, J.L. (1995) *Tropical Cyclone Formation. Global Perspectives on Tropical Cyclones*, (p. 289). Geneva: World Meteorological Organization. WMO/TD-No 693 (Ed. R. L. Elsberry), 501.

Montgomery, M.T., Nicholls, M.E., Cram, T.A. and Saunders, A.B. (2006) A vortical hot tower route to tropical cyclogenesis. *Journal of the Atmospheric Sciences*, 63, 355–386.

Montgomery, M.T., Lussier, L.L., Moore, R.W. and Wang, Z.W. (2010) The genesis of Typhoon Nuri as observed during the Tropical Cyclone Structure 2008 (TCS-08) field experiment. Part 1: the role of the easterly wave critical layer. *Atmospheric Chemistry and Physics*, 10, 9879–9900.

Montgomery, M.T. and Smith, R.K. (2011). Tropical-cyclone formation: theory and idealized modelling., *Proceedings of Seventh WMO International 503 Workshop on Tropical Cyclones (IWTC-VII), La ReUnion, Nov. 2010. (WWRP 2011-1)*. Geneva: World Meteorological Organization.

Montgomery, M.T., Davis, C., Dunkerton, T., Wang, Z., Velden, C., Torn, R., Majumdar, S.J., Zhang, F., Smith, R.K., Bosart, L., Bell, M.M., Haase, J.S., Heymsfield, A., Jensen, J., Campos, T. and Boothe, M.A. (2012) The Pre-Depression Investigation of Cloud Systems in the Tropics (PREDICT) Experiment: scientific basis, new analysis tools and some first results. *Bulletin of the American Meteorological Society*, 93, 153–172.

Montgomery, M.T. and Smith, R.K. (2014) Paradigms for tropical-cyclone intensification. *Australian Meteorlogical and Oceanographic Journal*, 64, 37–66.

Montgomery, M.T. and Smith, R.K. (2017) Recent developments in the fluid dynamics of tropical cyclones. *Annual Review of Fluid Mechanics*, 49, 1–33.

Morrison, H., Curry, J.A. and Khvorostyanov, V.I. (2005) A new double-moment microphysics parameterization for application in cloud and climate models. Part I: description. *Journal of the Atmospheric Sciences*, 62, 1665–1677.

Nguyen, S.V., Smith, R.K. and Montgomery, M.T. (2008) Tropical-cyclone intensification and predictability in three dimensions. *Quarterly Journal of the Royal Meteorological Society*, 134, 563–582.

Nolan, D.S. (2007) What is the trigger for tropical cyclogenesis?. *Australian Meteorological Magazine*, 56, 241–266.

Raymond, D.J. and Sessions, S.L. (2007) Evolution of convection during tropical cyclogenesis. *Geophysical Research Letters*, 34, L06811

Raymond, D.J., Sessions, S.L. and López Carillo, C. (2011) Thermodynamics of tropical cyclogenesis in the northwest Pacific. *Journal of Geophysical Research*, 116, D18101. https://doi.org/10.1029/2011JD015624

Raymond, D.J., Gjorgjievska, S., Sessions, S.L. and Fuchs, Z. (2014) Tropical cyclogenesis and mid-level vorticity. *Australian Meteorological and Oceanographic Society Journal*, 64, 11–25.

Rogers, R.F., Reasor, P.D., Zawislak, J.A. and Nguyen, L.T. (2020) Precipitation processes and vortex alignment during the intensification of a weak tropical cyclone in moderate vertical shear. *Monthly Weather Review*, 148, 1899–1929.

Rotunno, R. and Emanuel, K.A. (1987) An air-sea interaction theory for tropical cyclones. Part II evolutionary study using a nonhydrostatic axisymmetric numerical model. *Journal of the Atmospheric Sciences*, 44, 542–561.

Saunders, A.B. and Montgomery, M.T. (2004) *A Closer Look at Vortical Hot Towers within a Tropical Cyclogenesis Environment*. Colorado State University, Atmospheric Science. Bluebook No. 752.

Schlesinger, R.E. (1978) A three-dimensional numerical model of an isolated thunderstorm: Part I. Comparative experiments for variable ambient wind shear. *Journal of the Atmospheric Sciences*, 35, 690–713.

Smith, R.K. (2006) Accurate determination of a balanced axisymmetric vortex. *Tellus*, 58A, 98–103.

Smith, R.K. and Montgomery, M.T. (2012) Observations of the convective environment in developing and non-developing tropical disturbances. *Quarterly Journal of the Royal Meteorological Society*, 138, 1721–1739.

Smith, R.K. and Montgomery, M.T. (2016) Understanding hurricanes. *Weather*, 71, 219–223.

Tang, B.H., Rios-Berrios, R., Alland, J.J., Berman, J.D. and Corbosiero, K.L. (2016) Sensitivity of axisymmetric tropical cyclone spinup time to dry air aloft. *Journal of the Atmospheric Sciences*, 73, 4269–4287.

Tang, B.H., Fang, J., Bentley, A., Kilroy, G., Nakano, M., Park, M.S., Rajasree, V.P.M., Wang, Z., Wing, A.A. and Wu, L. (2020) Recent advances in research on tropical cyclogenesis. *Tropical Cyclone Research and Review*. https://doi.org/10.1016/j.tcrr.2020.04.004

Tao, C. and Jiang, H. (2015) Distributions of shallow to very deep precipitation – convection in rapidly intensifying tropical cyclones. *Journal of Climate*, 28, 8791–8824.

Terwey, W.D. and Rozoff, C.M. (2014) Objective convective updraft identification and tracking: Part 1. Structure and thermodynamics of convection in the rainband regions of two hurricane simulations. *Journal of Geophysical Research: Atmospheres*, 119, 6470–6496.

Tory, K. and Montgomery, M.T. (2006). Internal influences on tropical cyclone formation, *The Sixth WMO International Workshop on Tropical Cyclones (IWTC-VI)*. San José, CA. Geneva: World Meteorological Organization.

Tory, K. and Frank, W.M. (2010). Tropical cyclone formation. In J.D. Kepert and J.C.L. Chan (Eds.), *Chapter 2 of Global Perspectives on Tropical Cyclones: From Science to Mitigation, Series on Asia Pacific Weather and Climate 4*. Singapore: World Scientific.

Wang, Z., Montgomery, M.T. and Dunkerton, T.J. (2010) Genesis of pre-hurricane Felix (2007). Part I: the role of the easterly wave critical layer. *Journal of the Atmospheric Sciences*, 67, 1711–1729.

Wang, Z. (2014a) Role of cumulus congestus in tropical cyclone formation in a high-resolution numerical model simulation. *Journal of the Atmospheric Sciences*, 71, 1681–1700.

Wang, Z. (2014b) Characteristics of convective processes and vertical vorticity from the tropical wave to the tropical cyclone stage in the high-resolution numerical model simulations of tropical cyclone Fay (2008). *Journal of the Atmospheric Sciences*, 71, 896–915.

Wang, Z. (2018) What is the key feature of convection leading up to tropical cyclone formation?. *Journal of the Atmospheric Sciences*, 75, 1609–1629.

Weisman, M.L. and Klemp, J.B. (1982) The dependence of numerically simulated convective storms on vertical wind shear and buoyancy. *Monthly Weather Review*, 110, 504–520.

Wissmeier, U. and Smith, R.K. (2011) Tropical-cyclone convection: the effects of ambient vertical vorticity. *Quarterly Journal of the Royal Meteorological Society*, 137, 845–857.

Zawislak, J. and Zipser, E.J. (2014) A multisatellite investigation of the convective properties of developing and nondeveloping tropical disturbances. *Monthly Weather Review*, 142, 4624–4645.

Zawislak, J. (2020) Global survey of precipitation properties observed during tropical cyclogenesis and their differences compared to nondeveloping disturbances. *Monthly Weather Review*, 148, 1585–1606.

**How to cite this article:** Kilroy G. Evolution of convective characteristics during tropical cyclogenesis. *Q.J.R. Meteorol. Soc.*. 2021;147:2103–2123. https://doi.org/10.1002/qj.4011